White Rose Research Online

eprints@whiterose.ac.uk
https://eprints.whiterose.ac.uk
Universities of Leeds, Sheffield and York

Deposited via The University of Sheffield.

White Rose Research Online URL for this paper:
https://eprints.whiterose.ac.uk/id/eprint/172194/

Version: Published Version

Article:
Wu, X., Zhu, Z. and Wu, Z. (2021) A new simplified fundamental model-based sensorless control method for surface-mounted permanent magnet synchronous machines. IET Electric Power Applications, 15 (2). pp. 159-170. ISSN: 1751-8660

https://doi.org/10.1049/elp2.12022

Reuse
This article is distributed under the terms of the Creative Commons Attribution (CC BY) licence. This licence allows you to distribute, remix, tweak, and build upon the work, even commercially, as long as you credit the authors for the original work. More information and the full terms of the licence here: https://creativecommons.org/licenses/

Takedown
If you consider content in White Rose Research Online to be in breach of UK law, please notify us by emailing eprints@whiterose.ac.uk including the URL of the record and the reason for the withdrawal request.

UNIVERSITY OF LEEDS
University of Sheffield
UNIVERSITY of York

Received: 25 May 2020 | Revised: 3 August 2020 | Accepted: 11 September 2020

DOI: 10.1049/elp2.12022

IET Electric Power Applications

The Institution of Engineering and Technology WILEY

ORIGINAL RESEARCH PAPER

A new simplified fundamental model-based sensorless control method for surface-mounted permanent magnet synchronous machines

Ximeng Wu[1] | Zi-qiang Zhu[1] | Zhan-yuan Wu[2]

[1]Electronic and Electrical Engineering Department, University of Sheffield, Sheffield, UK

[2]Siemens Gamesa Renewable Energy Research Centre, University of Sheffield, Sheffield, UK

Correspondence

Zi-qiang Zhu, Electronic and Electrical Engineering Department, University of Sheffield, Sheffield S1 4DE, UK.
Email: z.q.zhu@sheffield.ac.uk

Funding information

UK EPSRC Prosperity Partnership, Grant/Award Number: EP/R004900/1

Abstract

For sensorless control of surface-mounted permanent magnet synchronous machines (SPMSMs), the major issue is in zero- and low-speed ranges. Since back-electromotive force (EMF) is proportional to speed, back-EMF based methods fail at zero and low speed. A solution considering the starting process and low speed sensorless control is presented. A simplified fundamental model-based method is proposed. Based on the simplified model, the measured stator currents in the stationary reference frame can be directly utilised for position estimation so that the sensorless control performance at low speed and starting is improved. Moreover, with the knowledge of rotor initial position sector information, a stable and reliable starting performance is achieved with the proposed method. The effectiveness of the proposed method is verified through experimental results.

1 | INTRODUCTION

In recent years, permanent magnet synchronous machines (PMSMs) are increasingly used in various applications due to their high torque density, power density and efficiency. Position sensorless control techniques become attractive because of their advantages including reduced cost and size, increased reliability, etc.

Basically, sensorless techniques can be divided into fundamental model-based techniques [1–12] and saliency tracking-based techniques [3–19]. Fundamental model-based methods utilising back-electromotive force (EMF) or flux-linkage have a good performance at middle and high speeds. Back-EMF and flux-linkage can be estimated simply using the phase-locked loop (PLL) or other observers including adaptive observer [4–6], sliding-mode observer (SMO) [7–10] and extended Kalman filter (EKF) [11,12]. However, the magnitude of back-EMF is proportional to the rotor speed, these methods present poor performance and cannot be employed in the zero- and low-speed range, whereas saliency tracking-based methods are more suitable in the zero- and low-speed range. Discrete voltage pulses [13], Pulse-width Modulation excitation [14] or continuous carrier signal injection-based methods [15–19] are proposed and show effectiveness in the zero- and low-speed range. However, in the case of surface-mounted permanent magnet synchronous machines (SPMSMs), due to geometric characteristics, the inductance saliency is insufficient or none. Hence, saliency tracking-based methods may not be employed for the SPMSM. Therefore, it is still a challenge for sensorless control of SPMSM at zero and low speed.

Conventionally, in order to employ sensorless control techniques on SPMSM, an open-loop start-up process [1,20–24] is adopted to help the machine first reach a certain high speed so that the magnitude of back-EMF is large enough for position tracking. However, with load or load variations, the operation may become unstable so that the machine will lose its synchronism. A reverse rotation or oscillation can also happen during starting. In addition, the starting torque is not guaranteed to be its maximum value, which will significantly slow down the starting process. Moreover, extra control strategies are required to achieve a smooth transition from open-loop control to closed-loop control [20–24].

A solution to SPMSM sensorless control considering the starting process and low speed operation is proposed. A simplified fundamental model based sensorless control method

This is an open access article under the terms of the Creative Commons Attribution License, which permits use, distribution and reproduction in any medium, provided the original work is properly cited.

© 2021 The Authors. *IET Electric Power Applications* published by John Wiley & Sons Ltd on behalf of The Institution of Engineering and Technology.

for SPMSM is proposed. Based on the simplified model, the stator currents in the stationary reference frame can be directly utilised for position estimation. Different from conventional fundamental model-based methods calculating back-EMF or flux-linkage, the proposed method utilises the rotor position information contained in the stator current. The stator currents are directly measured from the current sensors, and in the low-speed range, sensorless control performance can be improved. For the starting part, obtaining the accurate rotor initial position or sector information before starting is favourable in order to avoid the reverse rotation and oscillation issues that could possibly happen during starting [11,25]. Methods based on the magnetic saturation effect could be used [26,27]. A rotor initial position sector detection method in Ref. [26] is adopted, which guarantees a satisfactory estimation performance at standstill, especially for SPMSM. With the knowledge of the rotor initial sector, the proposed method is able to start the machine from standstill against different load conditions without reverse rotation. The influence of inverter nonlinearity on the proposed rotor position estimation method is also discussed, and the corresponding compensation is considered.

The study is organised into seven sections. In Section 2, conventional fundamental model-based sensorless control methods are introduced. Section 3 illustrates the proposed method including the mathematical model derivation, influence of inverter-nonlinearity and starting procedure. Finally, in Section 4, the proposed method is implemented on the dSPACE platform, and its effectiveness is verified by the experimental results on two prototype SPMSMs.

2 | CONVENTIONAL FUNDAMENTAL MODEL BASED SENSORLESS CONTROL METHOD

It is known that saliency tracking-based methods cannot be applied to SPMSM due to the lack of rotor saliency; fundamental model-based methods are the main way to realise sensorless control of SPMSM. For the fundamental model-based sensorless control methods [1–12], rotor position estimation is based on calculating either back-EMF or flux-linkage. In this part, the basic approaches of utilising back-EMF and flux-linkage for position estimation are demonstrated.

First, the fundamental model voltage equation in the stationary reference frame is given as:

$$\begin{bmatrix} v_\alpha \\ v_\beta \end{bmatrix} = \begin{bmatrix} R_s + pL_s & 0 \\ 0 & R_s + pL_s \end{bmatrix} \begin{bmatrix} i_\alpha \\ i_\beta \end{bmatrix} + \omega_r \psi_m \begin{bmatrix} -\sin\theta_r \\ \cos\theta_r \end{bmatrix} \tag{1}$$

where v_α, v_β and i_α, i_β are the stator voltages and currents in the stationary reference frame, respectively, R_s, L_s and ψ_m are the stator resistance, synchronous inductance and PM flux-linkage, respectively, ω_r, θ_r are the electrical rotor speed and the electrical rotor position, respectively, and p denotes the differential operator. The right hand side term represents the back-EMF that contains the rotor position and speed information. Back-EMF terms can be calculated as shown by Equation (2).

$$\begin{bmatrix} e_\alpha \\ e_\beta \end{bmatrix} = \begin{bmatrix} v_\alpha \\ v_\beta \end{bmatrix} - \begin{bmatrix} R_s + pL_s & 0 \\ 0 & R_s + pL_s \end{bmatrix} \begin{bmatrix} i_\alpha \\ i_\beta \end{bmatrix} \tag{2}$$

Then, the back-EMF terms are given as

$$\begin{bmatrix} e_\alpha \\ e_\beta \end{bmatrix} = \omega_r \psi_m \begin{bmatrix} -\sin\theta_r \\ \cos\theta_r \end{bmatrix} \tag{3}$$

The rotor position can be calculated by

$$\theta_r = \arctan\left(-\frac{e_\alpha}{e_\beta}\right) \tag{4}$$

Another conventional way is to calculate the flux-linkage which is actually the integration of back-EMF. The flux-linkage can be calculated as follows:

$$\psi_{m,\alpha\beta} = \int (v_{\alpha\beta} - R_s i_{\alpha\beta}) dt - L_s i_{\alpha\beta} \tag{5}$$

The flux-linkages are given as

$$\begin{bmatrix} \psi_{m\alpha} \\ \psi_{m\beta} \end{bmatrix} = \psi_m \begin{bmatrix} \cos\theta_r \\ \sin\theta_r \end{bmatrix} \tag{6}$$

The rotor position can be obtained as

$$\theta_r = \arctan\frac{\psi_{m\beta}}{\psi_{m\alpha}} \tag{7}$$

It is obvious that conventional methods based on the fundamental model offer good performance in the middle- and high-speed ranges. While in zero- and low-speed ranges, back-EMF and flux-linkage are unobservable, besides there are also some other factors affecting the sensorless control performance including the parameter mismatch, inverter non-linearity, etc. Therefore, the conventional fundamental model-based methods normally cannot be used in zero- and low-speed ranges. In order to solve this issue, a new sensorless control method based on the simplified fundamental model is proposed.

3 | PROPOSED SIMPLIFIED FUNDAMENTAL MODEL BASED SENSORLESS CONTROL METHOD

Based on the fundamental model in Section 2, a new simplified fundamental model-based sensorless control method is introduced in this section. Instead of calculating back-EMF or flux-linkage in conventional ways, only the measured stator currents are directly used to extract the rotor position information in the proposed method. Since currents are measured from physical sensors, comparing with conventional direct utilization of back-EMF or flux-linkage, the sensorless control performance can be improved in starting and low-speed range. In this section, the mathematical model derivation of the proposed simplified fundamental model is provided at first including the demonstration of how to utilise stator current to estimate the rotor position. Furthermore, the influence of inverter nonlinearity is discussed. The overall sensorless control block diagram is illustrated in Figure 1.

3.1 | Mathematical model

The proposed method is based on the fundamental model given in Equation (1). However, in the sensorless control system, the real rotor position is unknown initially, and therefore, the voltage Equation (1) should be transformed into the estimated reference frame by using the transformation matrix in Equations (8) and (9).

$$T(\Delta\theta_r) = \begin{bmatrix} \cos\Delta\theta_r & -\sin\Delta\theta_r \\ \sin\Delta\theta_r & \cos\Delta\theta_r \end{bmatrix} \tag{8}$$

$$T^{-1}(\Delta\theta_r) = \begin{bmatrix} \cos\Delta\theta_r & \sin\Delta\theta_r \\ -\sin\Delta\theta_r & \cos\Delta\theta_r \end{bmatrix} \tag{9}$$

where $\Delta\theta_r$ is the position error between the actual position and the estimated position. Then, the d-axis voltage in the estimated reference frame can be represented as:

$$\hat{v}_d = R_s\hat{i}_d + L_s\frac{d\hat{i}_d}{dt} - \omega_r L_s\hat{i}_q - \hat{E}_d \tag{10}$$

where $\hat{E}_d = \omega_r\psi_m\sin\Delta\theta_r$, neglecting the transient part which is relatively small. Then, the Equation (10) becomes:

$$\hat{v}_d = R_s\hat{i}_d - \omega_r L_s\hat{i}_q - \hat{E}_d \tag{11}$$

A d-axis voltage command is given by:

$$\hat{v}_d = -\omega_r L_s\hat{i}_q \tag{12}$$

Under this condition, Equation (11) is simplified as:

$$R_s\hat{i}_d = \hat{E}_d = \omega_r\psi_m\sin\Delta\theta_r \tag{13}$$

Since the position error $\Delta\theta_r$ is directly proportional to the d-axis current in Equation (13), the estimated d-axis current can be directly utilised as the input of a position observer. The position error $\Delta\theta_r$ will be forced to zero by the observer, and the estimated reference frame will align with the actual one. Moreover, in Figure 2a, the phasor diagram of the proposed method indicates that the current will be aligned with the back-EMF vector. Hence, the rotor position can be estimated directly by the stator current.

Based on Equation (13), and the rotor position can be estimated by a phase-locked loop (PLL) as shown in Figure 3.

The PLL used here is a conventional and common way to extract phase and frequency information from input signals. The input error of PLL is represented as:

$$\hat{i}_d = \cos\hat{\theta}_r i_\alpha + \sin\hat{\theta}_r i_\beta = \varepsilon_{PLL} \tag{14}$$

After the error ε_{PLL} converges to zero, the position will be tracked, and position estimation error is zero, that is $\Delta\theta_r = 0$.

More importantly, since this study is focused on the low speed range, it is assuming that the value of $\omega_r L_s$ is small, and the d-axis voltage command can be simplified as:

$$\hat{v}_d \approx 0 \tag{15}$$

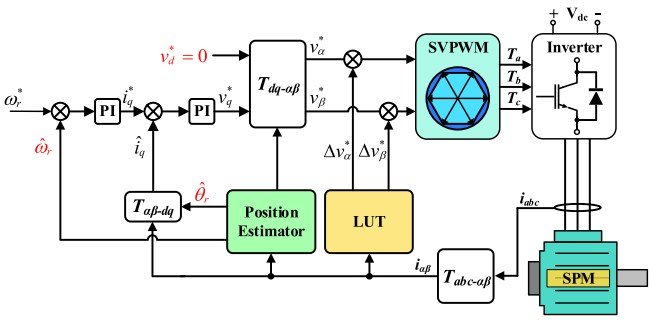

FIGURE 1 Overall sensorless control block diagram

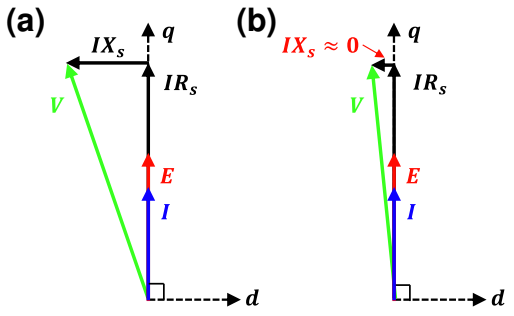

FIGURE 2 Phasor diagram of permanent magnet synchronous machines (PMSM). (a) High speed, (b) Low speed

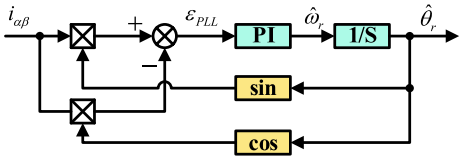

FIGURE 3 Block diagram of phase-locked loop

It is also demonstrated by Figure 2b that the d-axis voltage is approximately zero at low speed. Clearly, this simplification makes the estimation algorithm simpler and becomes quasi non-parametric at lower speed. It is worth noting that the simplification from Equations (12)–(15) can bring estimation errors at higher speed, especially under load conditions, and thus, it is necessary to compensate d-axis voltage at high speed. Since the low speed range is mainly focused, the compensation is not necessary.

Overall, the proposed method simplifies the estimation process so that the rotor position can be directly extracted from stator current at low speed through a PLL or other observers, without the need of machine parameters. More importantly, the current information is provided by the current sensor. Thus, a good estimation performance is expected, especially in the low speed range. This benefit makes this proposed method effective and capable of position estimation in the low speed range and even starting from the standstill.

3.2 | Phase-locked loop

As discussed in Section 3.1, a quadrature PLL is used to track the rotor position information from the stator currents. Based on Equation (14), the equivalent block diagram of PLL is shown in Figure 4.

In Figure 4, $k = \sqrt{i_\alpha^2 + i_\beta^2}$ which varies with different conditions. In order to fix the poles of the PLL transfer function at different conditions, it is necessary to normalise the input signals by dividing k. Then, the normalised input error signal of PLL can be expressed as:

$$\varepsilon_{PLL,N} = \frac{1}{\sqrt{i_\alpha^2 + i_\beta^2}}\left(i_\alpha \cos\hat{\theta}_r + i_\beta \sin\hat{\theta}_r\right) \tag{16}$$

Therefore, the closed loop transfer function of the PLL can be given by

$$H(s) = \frac{K_p s + K_i}{s^2 + K_p s + K_i} \tag{17}$$

Equation (17) can be re-arranged as:

$$H(s) = \frac{2\xi\omega_n s + \omega_n^2}{s^2 + 2\xi\omega_n s + \omega_n^2} \tag{18}$$

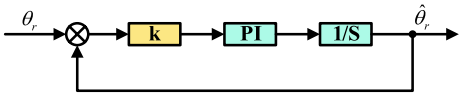

FIGURE 4 Equivalent block diagram of phase-locked loop

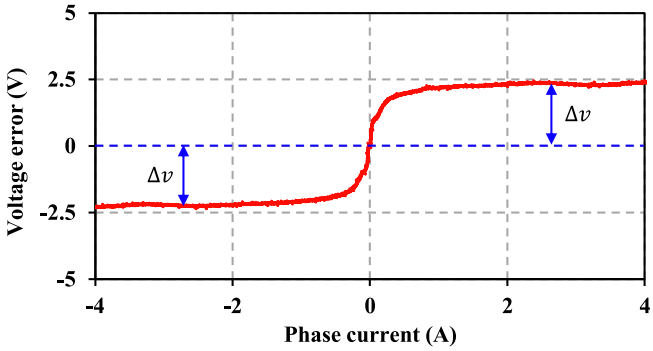

FIGURE 5 Measured voltage error against phase current

where $\omega_n = \sqrt{K_i}$, $\xi = \frac{K_p}{2}\sqrt{\frac{1}{K_i}}$. ω_n is the natural frequency and can be used as the bandwidth of PLL. ξ is the damping factor. A higher damping factor can reduce the overshoot but also sacrifice the dynamic performance. Then, the parameters of PLL can be initially designed. Furthermore, the stability of PLL should also be considered after determining the parameters of PLL. Since the PLL used is a typical second-order PLL, according to Ref. [28], this type of PLL is unconditionally stable for all positive values of parameters.

3.3 | Inverter nonlinearity effect

As mentioned in Section 3.1, in order to make θ_v zero, a zero command is given to d-axis voltage, which is shown in Figure 1. However, it is worth noting that in practice, the output voltage of the inverter may be different from the reference voltage due to inverter-nonlinearity, of which the dead-time is the main contribution to the output voltage error. Two SPMs are tested, and SPM-I is taken as the example; the influence of inverter-nonlinearity on the proposed position estimation method is investigated.

According to References [29–31], the relationship between voltage error and current can be obtained due to inverter-nonlinearity. Then, the voltage error against the current is measured and shown in Figure 5. It can be seen that the voltage error is relatively small compared to the rated terminal voltage of the tested SPMSM as shown in Table I. The sampling frequency and dead time settings of the test rig are 2.5 kHz and 2μs, respectively.

Equation (19) illustrates that the actual d-axis voltage is different from the reference due to inverter-nonlinearity.

$$v_d^* = v_d + \Delta v_d \tag{19}$$

TABLE 1 Parameters of test SPMSM machines

Variable name	SPM-I	SPM-II
DC-link voltage (V)	230	40
Rated current (A, peak)	4	4
Rated torque (Nm)	91	2.1
Rated speed (rpm)	170	400
Pole pairs	16	5
Stator resistance (Ω)	4	1.096
PM flux-linkage (Wb)	0.9	0.07
Synchronous inductance (mH)	17.21	2.31
Inertia (kg·m^2)	2.6	0.002

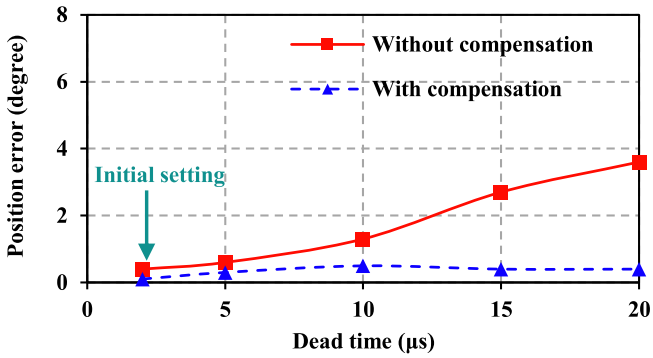

FIGURE 6 Position estimation error against dead-times

As mentioned in Section 3.1 before, θ_v is controlled to zero. Due to the existence of Δv_d, an error is therefore introduced in the angle θ_v, which is shown in Equation (20).

$$\Delta\theta_v = arctan\frac{\Delta v_d}{v_q} \tag{20}$$

Based on the mathematical model in Part A, a non-zero θ_v will cause a position estimation error. However, it is obviously seen from Equation (20) that a slight difference in v_d can be minimised by dividing v_q. In all, as shown in Figure 6, with the original settings of dead time and switching frequency, position estimation error caused by this inverter nonlinearity can be ignored. Therefore, the compensation of inverter-nonlinearity may be unnecessary.

However, if the inverter-nonlinearity effect becomes more significant, then the estimation error will increase so that it cannot be ignored as before. Therefore, corresponding compensations are necessary. In Figure 6, the dead-time is intentionally increased to investigate its influence on position estimation error. Clearly, it can be seen that position error increases as the dead-time becomes larger.

There are many methods [29–31] to solve the influence of inverter-nonlinearity effect, with which the influence can be solved properly. Based on the relationship between the measured voltage errors against current shown in Figure 5, a compensation Look-up Table (LUT) is generated to solve the position estimation error due to inverter nonlinearity. The generated compensation LUT can be represented as a nonlinear function between the output voltage error and the phase current. This nonlinear function can be represented by

$$\Delta v = g(i) \tag{21}$$

Then, the voltage command is modified to:

$$v^{**} = v^{*} + g(i) \tag{22}$$

The block diagram of the compensation is shown in Figure 1. Figure 6 shows that after compensation, the position error caused by inverter-nonlinearity is eliminated apparently.

3.4 | Starting procedure

For conventional fundamental model-based methods, zero- and low-speed sensorless control performance is poor due to non-observable back-EMF. For the proposed method, the stator currents are directly used to estimate the position, and the low speed sensorless control performance could be improved. Although for the proposed method, zero-speed rotor position estimation is unfeasible, it is still possible to start the machine as long as the observer can quickly converge to the actual position after an initial rotation movement is seen without the knowledge of rotor initial position information, the starting performance may not be satisfactory and become even worse, for example reverse rotation issue [11,25], which is not allowed by some applications. In Reference [11], a countermeasure to reverse rotation during starting is proposed by looking at the estimated speed, and a 180-degree compensation angle is compensated during reverse rotation. However, a large q-axis current impulse will be produced during the correction, producing harmful torque. Hence, before starting the rotor initial position information is obtained to improve the starting performance and prevent the reverse rotation. Rotor initial position estimation methods based on magnetic saturation effect [26,27] are a satisfactory alternative and are employed.

The method described in Reference [26] is adopted to estimate the rotor initial sector. By using method described in Reference [26], initial rotor position can be estimated with a maximum error of 15°. With the knowledge of the rotor initial position sector, a more reliable starting performance can be achieved without reverse rotation, which will be verified by experimental results.

4 | EXPERIMENTAL RESULTS

The experiments are implemented on the dSPACE platform to validate the effectiveness of the proposed method on two prototype SPM machines (Their parameters are shown in

Table I). In Table I, although SPM-I has a larger PM flux-linkage, the larger inertia makes it more difficult to start up. SPM-II has a much smaller inertia but its PM flux-linkage is also much smaller than SPM-I. The overall platforms of SPM-I and SPM-II are shown in Figure 7. For both test rigs, a three-phase voltage source inverter (VSI) and a DC power supply are included in the experimental setup. The stator currents are measured through Hall Effect sensors. Both prototype SPMSM machines are equipped with encoders for comparison with the estimated position. As shown in Figure 7a, a torque motor is connected to the tested SPM-I through the shaft. The torque motor can be operated in torque control mode to provide the desired load to the tested SPM-I.

In the experiment section, first, the operation points of the proposed method compared with Maximum torque per ampere (MTPA) curve are shown. Then, the influence of model simplification on position estimation error considering different load and speed is investigated. Afterwards, both steady- and dynamic-state position estimation performances are investigated. Moreover, the starting performance test is also carried out. At last, the current measurement error and parameter variations on position estimation are analysed.

4.1 | Comparison with MTPA operation

As illustrated in Section 3.1, the proposed method is based on a simplified model, and a small amount of d-axis current will exist. Hence, the MTPA operation may not be guaranteed, taking SPM-I as an example. Figure 8 shows the tested operation points with the proposed method and MTPA curve at different speed. It can be seen that as load or speed increases, the operation point goes further than the MTPA curve. This is due to the model simplification from Equations (12)–(15). Nevertheless, at the rated load condition in lower speed range, the output torque reduction is small so that it can be neglected.

4.2 | Influence of model simplification

As illustrated in Section 3.1, the proposed method is based on a simplified model at low speed. Hence, the influence of this simplification on position error considering different load and speed is carried out. Take SPM-I as example since the load can be simply controlled. Figure 9 shows the average position errors against different rotor speed and load.

From Figure 9, it is seen that as speed increases, the estimation error increases as well, and the error will also increase with load. Hence, the proposed method is preferred in a lower speed range. At low speed, the position error can be neglected considering different load conditions.

4.3 | Steady-state performance

The steady-state sensorless control performance with the proposed method is illustrated in Figures 10–13. The position

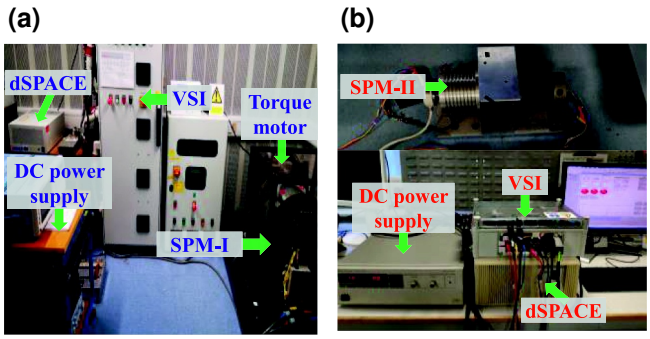

FIGURE 7 Test rig. (a) SPM-I, (b) SPM-II

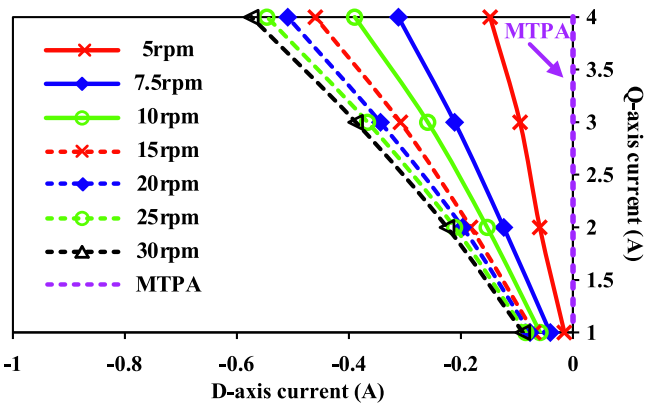

FIGURE 8 Comparison with MTPA operation points. MTPA, Maximum torque per ampere.

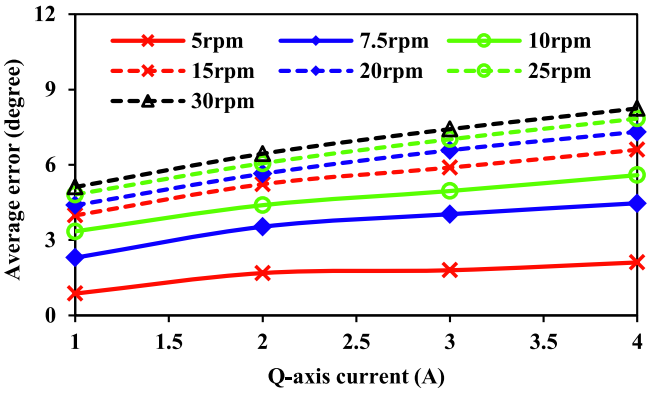

FIGURE 9 Average position estimation error against rotor speed and load

estimation error is $\Delta\theta_r$. In the test, SPM-I and SPM-II are controlled at 5 and 25 rpm, respectively, which are approximately the minimum speeds that give the reliable performance. For both SPM-I and SPM-II, the no load steady-state performance is shown in Figures 10 and 11, and the full load ones are shown in Figures 12 and 13. It can be seen that the proposed method provides good performance with different load conditions at a low speed. Moreover, as shown in Figure 14, the machine is operating at 25 rpm with the proposed method at first, and then, the sensorless algorithm is switched to the

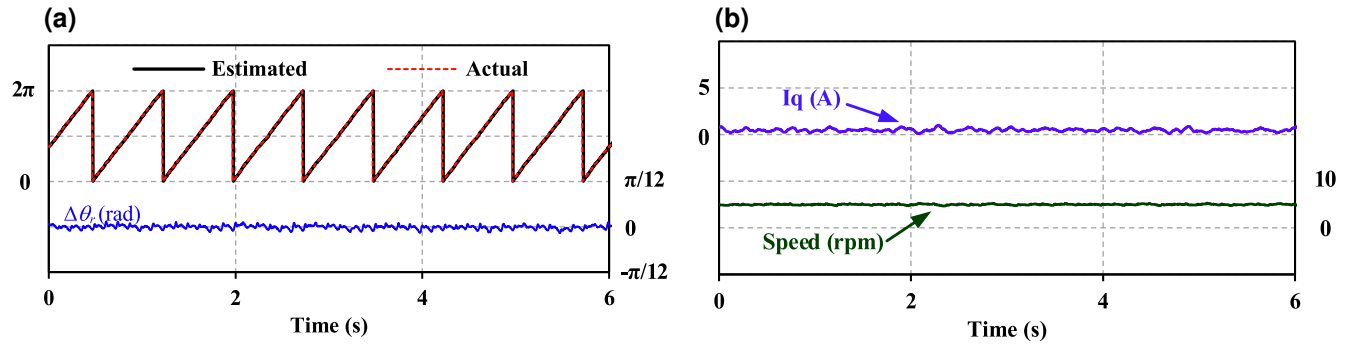

FIGURE 10 No load steady-state performance at 5 rpm (SPM-I). (a) Rotor position estimation, (b) Rotor speed and q-axis current

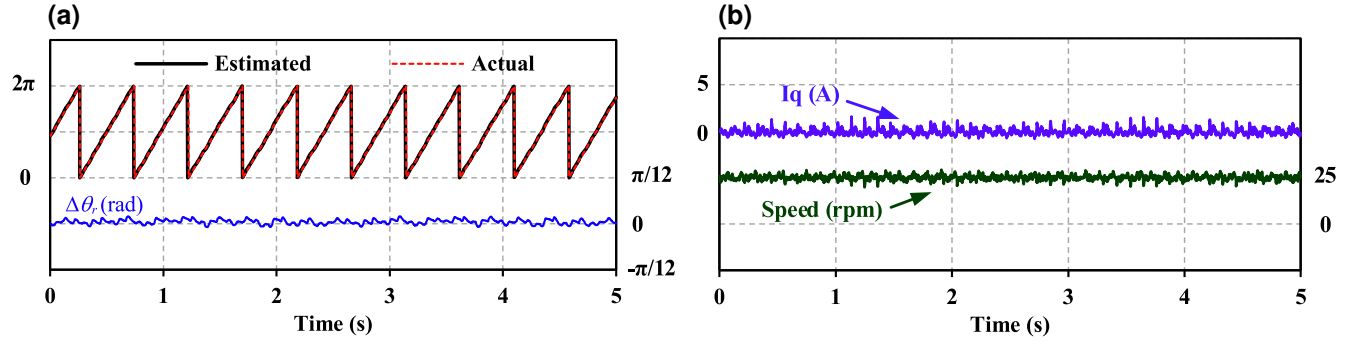

FIGURE 11 No load steady-state performance at 25 rpm (SPM-II). (a) Rotor position estimation, (b) rotor speed and q-axis current

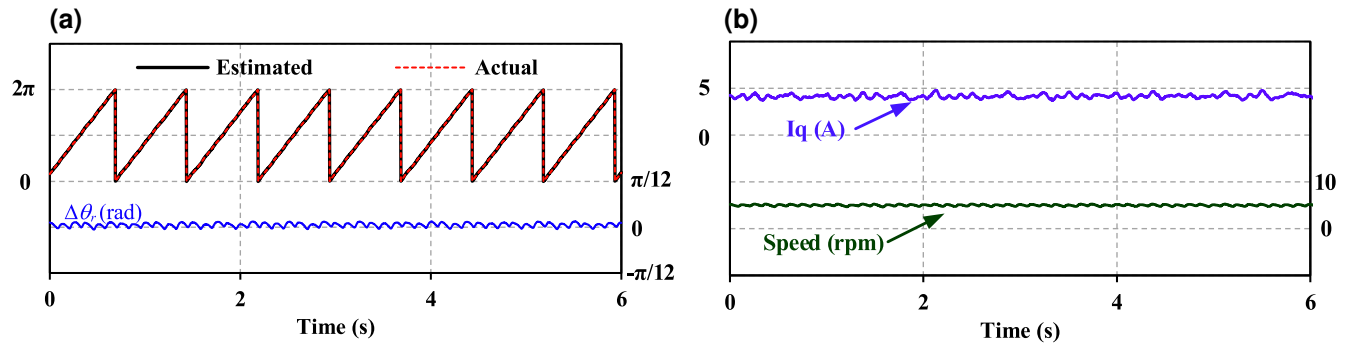

FIGURE 12 Full load steady-state performance at 5 rpm (SPM-I). (a) Rotor position estimation, (b) rotor speed and q-axis current

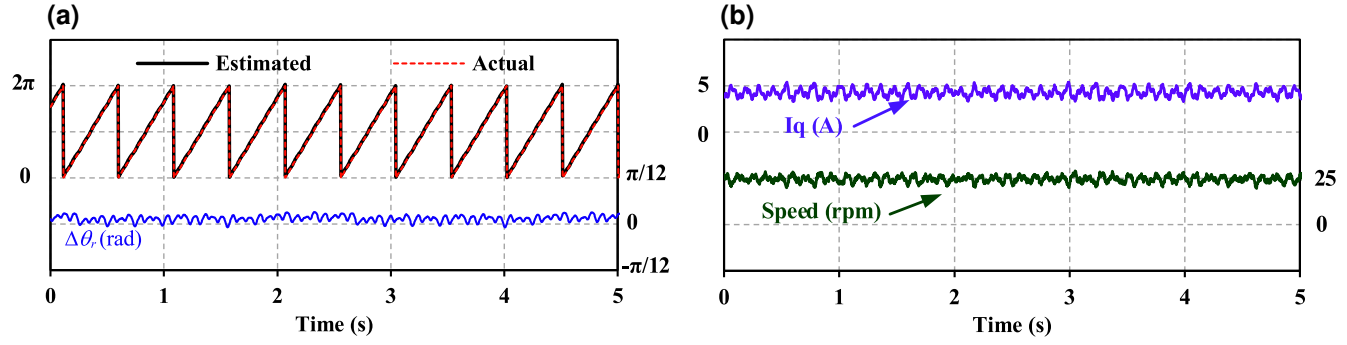

FIGURE 13 Full load steady-state performance at 25 rpm (SPM-II). (a) Rotor position estimation, (b) rotor speed and q-axis current

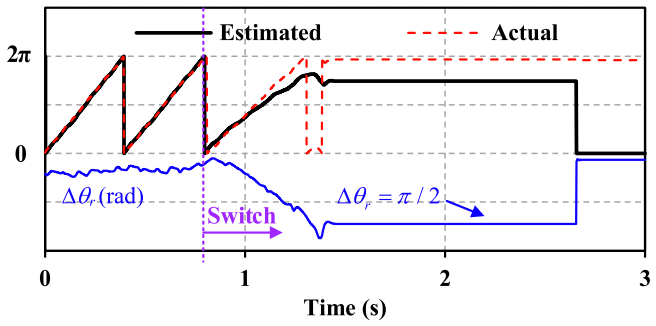

FIGURE 14 Sensorless operation switching from proposed method to the conventional method [2]

conventional method [2]. It is found that after switching methods, the sensorless operation cannot be sustained.

4.4 | Dynamic-state performance

The dynamic performance of the proposed method is also presented in this part. For both SPM-I and SPM-II, step speed and step load tests are carried out. For the step speed test on SPM-I in Figure 15, the speed reference is given as 0–10–20 rpm. For the step speed test on SPM-II in Figure 16, the speed reference is given as 20–50–100–200 rpm. From the result, it can be observed that the rotor is able to start from standstill well and then follow the given speed reference properly with the proposed method. Then, the step load test of both SPM-I and SPM-II is shown in Figures 17 and 18. It is shown that the proposed method gives a good position tracking performance when q-axis current changes rapidly from no-load to full-load. In all, it can be concluded that the proposed position estimation method presents a satisfactory dynamic performance.

4.5 | Starting performance

In this part, starting performance is examined. First, in Figure 19a, a starting failure using the conventional back-EMF based method [2] is shown. Next, as discussed in Section III, the rotor initial sector information can be favourable in a reliable starting performance. Figure 19b shows the starting performance without the knowledge of rotor initial sector information, and it can be seen that a reverse starting happens.

In contrast, with the knowledge of rotor initial sector, starting performance is tested. Rotor initial sector is first estimated based on Reference [26]. The maximum initial position error is 15°. Therefore, in this part, the machine starts from standstill to the reference speed with 15° initial position error. Figures 20 and 21 show the starting performance with the proposed method considering no-load conditions on both test machines. For the no-load test, it can be seen that the position can be tracked quickly and gives a satisfactory starting performance. In case of starting with full-load, due to hardware limitation, the test is only carried out on SPM-I. The torque motor is set as zero speed with a 91 Nm torque limit which is the rated torque of the SPM-I. As long as the SPM-I can provide a proper torque that is larger than 91 Nm during starting, the machine can start to accelerate to the reference speed. As shown in Figure 22, the proposed method is able to start the machine from standstill with full-load.

4.6 | Current measurement error

Since the stator current is directly used for position estimation of the proposed method. The influence of current measurement error including gain error and dc offset error is investigated in this section.

First, the measured three-phase current are expressed by.

$$\begin{bmatrix} i_A' \\ i_B' \\ i_C' \end{bmatrix} = \begin{bmatrix} i_A \\ i_B \\ i_C \end{bmatrix} + \begin{bmatrix} \Delta i_A \\ \Delta i_B \\ \Delta i_C \end{bmatrix} \tag{23}$$

$$\begin{bmatrix} \Delta i_A \\ \Delta i_B \\ \Delta i_C \end{bmatrix} = \begin{bmatrix} (k_a - 1) i_A \\ (k_b - 1) i_B \\ -(k_a - 1) i_A - (k_b - 1) i_B \end{bmatrix} + \begin{bmatrix} \delta_A \\ \delta_B \\ -\delta_A - \delta_B \end{bmatrix} \tag{24}$$

where i_A', i_B' and i_C' are the measured currents, i_A, i_B and i_C are the real currents, and Δi_A, Δi_B and Δi_C are the current measurement errors. k_a and k_b indicate the gains of the phase A and B currents, and they are unity if there is no gain error. δ_A and δ_B are the DC offsets of phase A and B currents, and they are zero when there are no DC offset errors. Besides, it is assumed that for a star connection drive system, phase A and B currents are measured and phase C current is calculated.

Then, according to Reference [32], it is known that the gain error will cause DC and second order harmonics in the estimated position. The DC offset error will produce a synchronous frequency component in the estimated position. Experiments results are shown in Figure 23 including the position estimation errors with DC offset error and gain error. Comparison with the conventional back-EMF based method [2] is also shown in Figure 23.

In Figure 23, different sets of gain errors and dc offset errors are considered. According to experiment results, it is found that the proposed method is more sensitive to current measurement error compared with conventional back-EMF based method. This is due to the fact that the current in the stationary reference frame is directly used for position estimation. Nevertheless, the current sensors are normally calibrated in the pre-test, and hence, the DC offset and gain errors are minimised. Therefore, their influence on the position estimation can be eliminated.

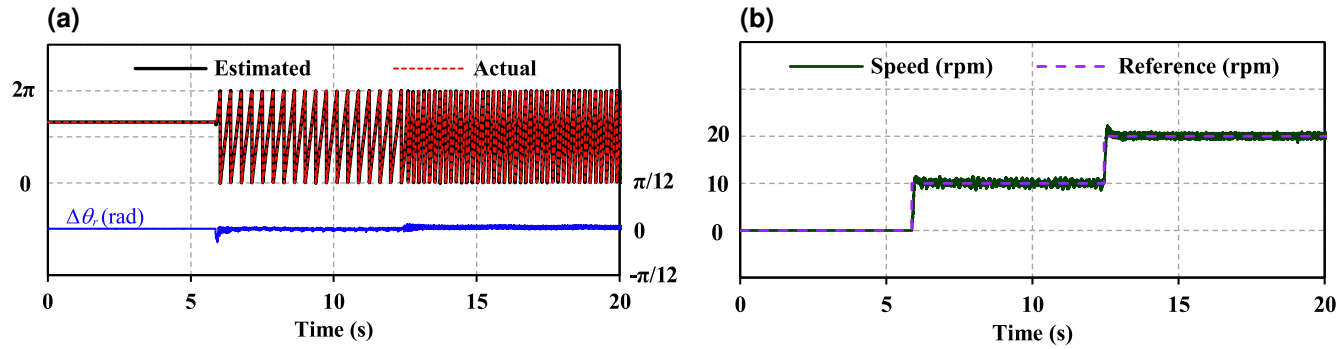

FIGURE 15 Dynamic performance under step speed (SPM-I). (a) Rotor position estimation, (b) Rotor speed and speed reference

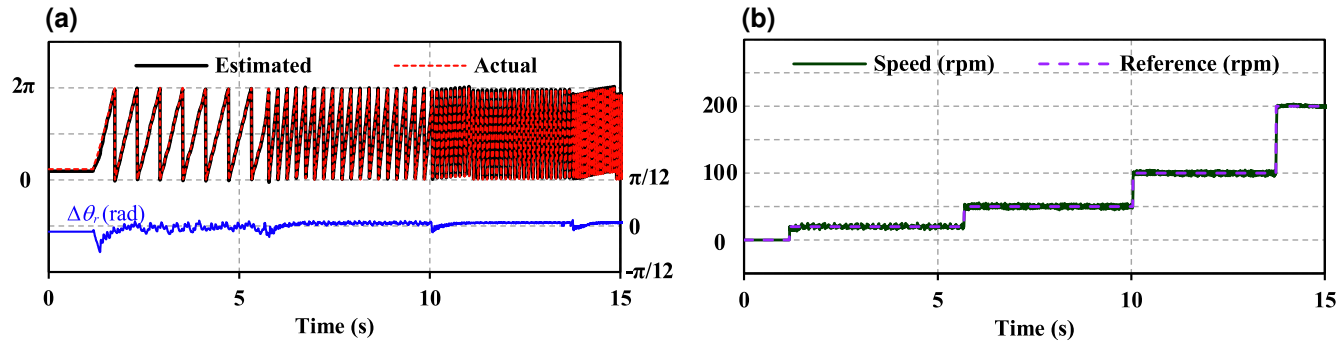

FIGURE 16 Dynamic performance under step speed (SPM-II). (a) Rotor position estimation, (b) Rotor speed and speed reference

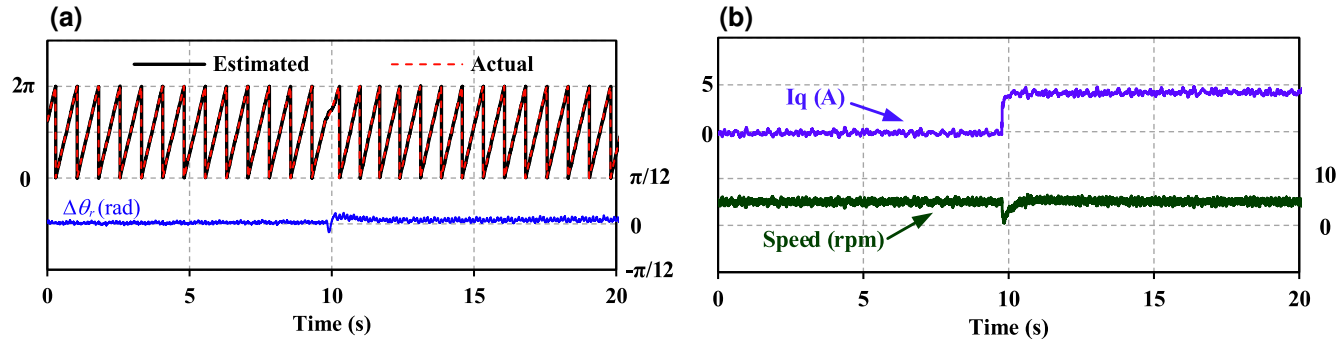

FIGURE 17 Dynamic performance under step load (SPM-I). (a) Rotor position estimation, (b) rotor speed and *q*-axis current

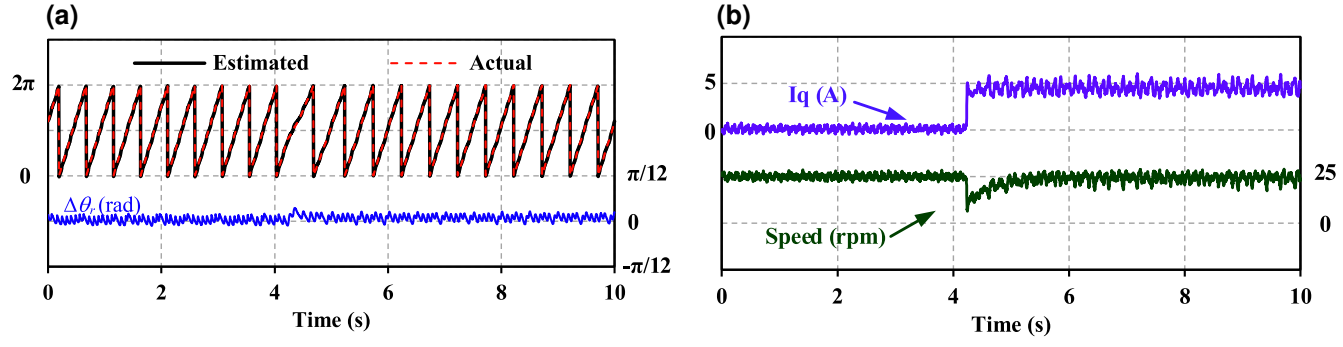

FIGURE 18 Dynamic performance under step load (SPM-II). (a) Rotor position estimation, (b) Rotor speed and *q*-axis current

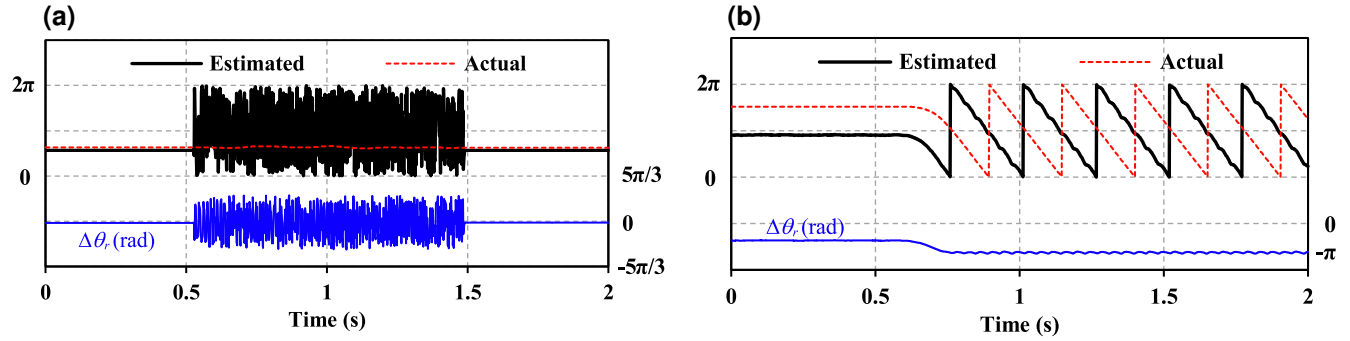

FIGURE 19 Starting failure cases with the conventional back-electromagnetic force (EMF) method [2]. (a) Conventional back-EMF method [2], (b) proposed method without knowledge of rotor initial sector

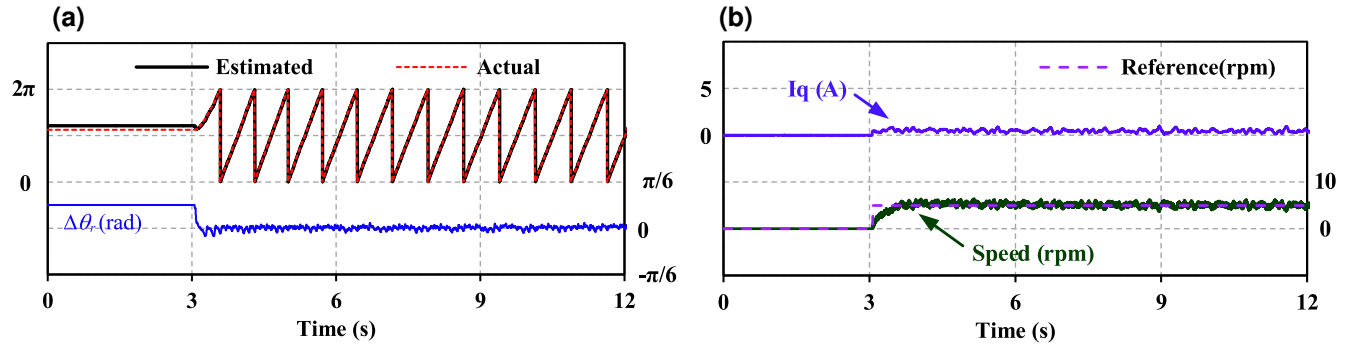

FIGURE 20 Starting performance with no-load, with knowledge of rotor initial sector information. (SPM-I) (a) Rotor position estimation, (b) Rotor speed and q-axis current

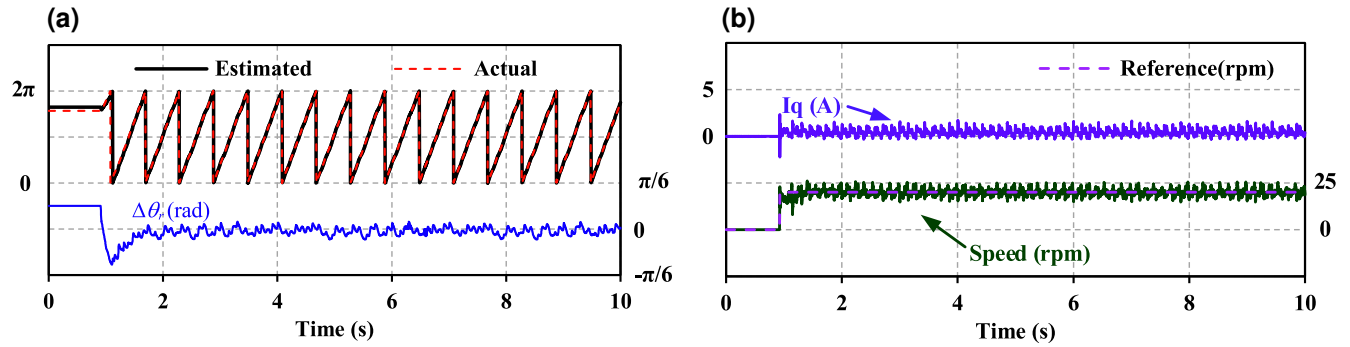

FIGURE 21 Starting performance with no-load, with knowledge of rotor initial sector information. (SPM-II) (a) Rotor position estimation, (b) Rotor speed and q-axis

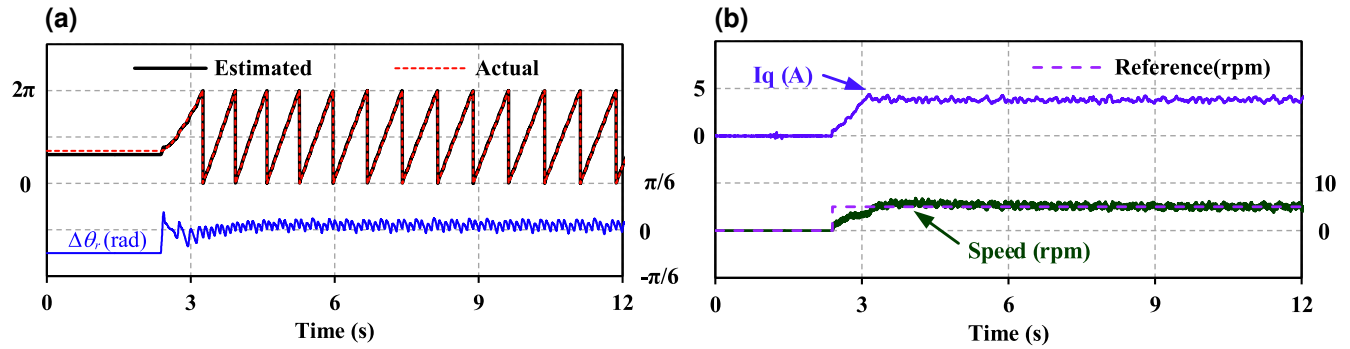

FIGURE 22 Starting performance with full-load, with knowledge of rotor initial sector information. (SPM-I) (a) Rotor position estimation. (b) Rotor speed and q-axis current

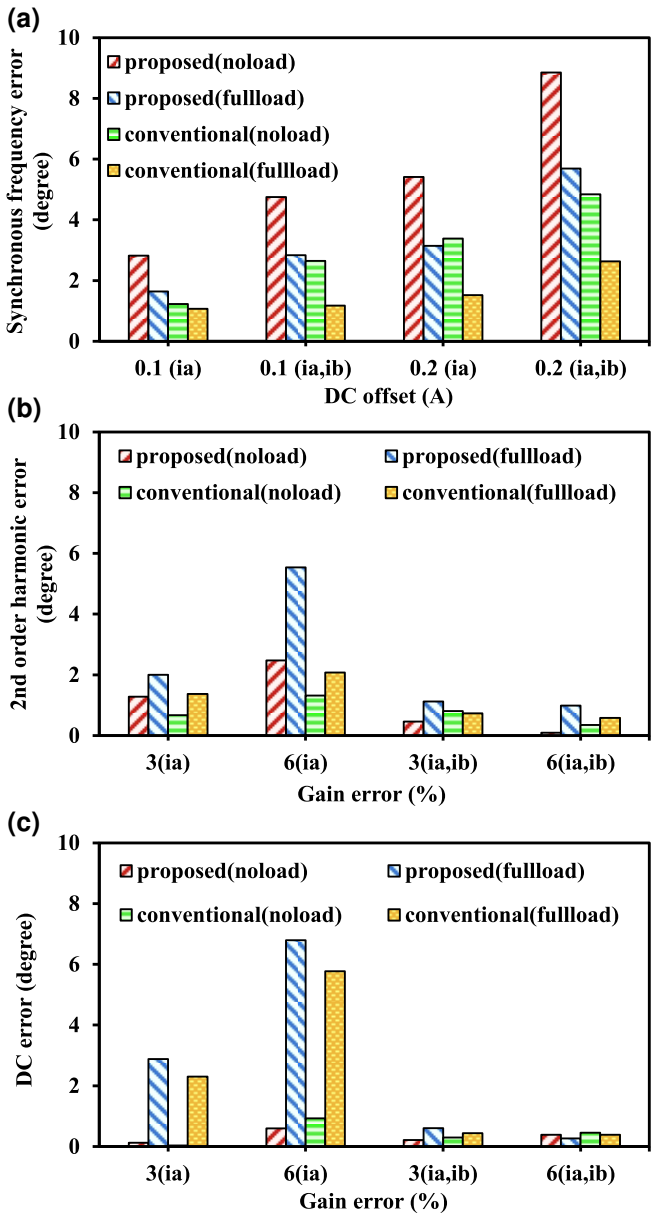

FIGURE 23 Position error with current measurement errors. (a) Synchronous frequency component with DC bias error, (b) second order harmonic frequency component with gain error, (c) DC component with gain error

4.7 | Parameter sensitivity

The parameter sensitivity including resistance and inductance are investigated in this section. Figure 24 shows the experimental results of estimation error against parameter mismatches at 10 rpm.

For the resistance, the proposed method is not influenced by resistance mismatch. According to the mathematic model of the proposed method, the estimated position error is directly proportional to the estimated d-axis current which is given by:

$$R_s\hat{i}_d = \hat{E}_d = \omega_r\psi_m \sin\Delta\theta_r \tag{25}$$

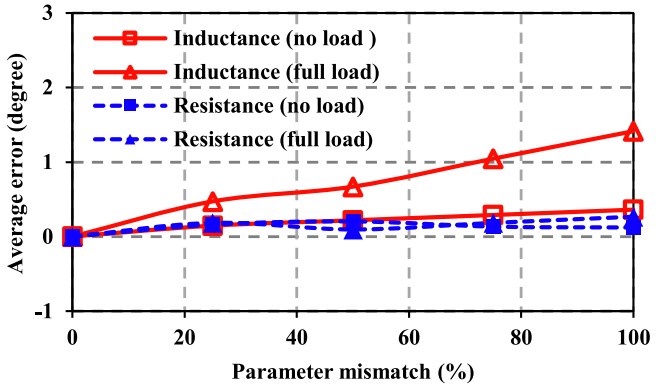

FIGURE 24 Position error with parameter mismatch

The observer will force the d-axis current to zero so that the position error $\Delta\theta_r$ is zero. The value of resistance will not affect the position error. As shown in Figure 24, the position error is not related to the resistance.

For the inductance, the proposed method assumes that the d-axis voltage is zero at lower speed which is represented in Equation (26).

$$\hat{v}_d = -\omega_r L_s \hat{i}_q \approx 0 \tag{26}$$

The influence of inductance is related to the q-axis current. From Figure 24, it can be seen that under full load, the estimation error becomes more sensitivity to inductance changes. Nevertheless, the position error is small when inductance is 100% mismatch, the torque reduction (≈0.01% of rated value) could be acceptable.

5 | CONCLUSION

A simplified fundamental model-based sensorless control method is proposed for SPMSM in the low speed range and considering the starting process. Instead of calculating back-EMF or flux-linkage as conventional methods, the proposed method directly uses stator currents in the stationary reference frame for rotor position estimation, providing a more effective way to estimate the rotor position. A good position estimation performance at low speed is achieved since the current information is directly obtained from the current sensors. Moreover, with the knowledge of the rotor initial sector before starting, the proposed method is able to provide a satisfactory starting performance even with the load. The proposed methods are verified through experimental results, showing good position estimation performance under different operations.

Meanwhile, the limitations of the proposed method are summarised as follows:

1. Since the model is simplified, at higher speed, the position estimation error will increase, especially under load conditions. Therefore, the proposed method is preferred to be applied in the low speed range.

2. MTPA condition is not guaranteed, since the model is simplified, and therefore, a small amount of *d*-axis current exists. While in the low speed range, the torque reduction is neglectable.
3. The proposed method is more sensitive to current measurement errors than the conventional back-EMF based method. Hence, the current sensor should be calibrated properly in the pre-test.

Since the proposed method provides a good performance for SPMSM for starting and in the low speed range, it may be combined with the conventional method at medium and high speeds to provide a good performance over the whole operating speed range.

ACKNOWLEDGEMENTS

This work was supported by UK EPSRC Prosperity Partnership 'A New Partnership in Offshore Wind' under Grant No. EP/R004900/1.

ORCID

Ximeng Wu https://orcid.org/0000-0002-8111-3191

REFERENCES

1. Wu, R., Slemon, G.R.: A permanent magnet motor drive without a shaft sensor. IEEE Trans. Ind. Appl. 27(5), 1005–1011 (1991)
2. Chen, Z., et al.: An extended electromotive force model for sensorless control of interior permanent-magnet synchronous motors. IEEE Trans. Ind. Electron. 50(2), 288–295 (2003)
3. Genduso, F., et al.: Back EMF sensorless-control algorithm for high-dynamic performance PMSM. IEEE Trans. Ind. Electron. 57(6), 2092–2100 (2010)
4. Piippo, A., Hinkkanen, M., Luomi, J.: Analysis of an adaptive observer for sensorless control of interior permanent magnet synchronousmotors. IEEE Trans. Ind. Electron. 55(2), 570–576 (2008)
5. Yoo, A., Sul, S.K.: Design of flux observer robust to interior permanent-magnet synchronous motor flux variation. IEEE Trans. Ind. Appl. 45(5), 1670–1677 (2009)
6. Yao, Y., et al.: Position sensorless drive and online parameter estimation for surface-mounted PMSMs based on adaptive full-state feedback control. IEEE Trans. Power Electron. 35(7), 7341–7355 (2020)
7. Chi, S., Zhang, Z., Xu, L.: Sliding-mode sensorless controlof direct-drive PM synchronous motors for washing machine applications. IEEE Trans. Ind. Appl. 45(2), 582–590 (2009)
8. Kim, H., Son, J., Lee, J.: A high-speed sliding-mode observer for the sensorless speed control of a PMSM. IEEE Trans. Ind. Electron. 58(9), 4069–4077 (2011)
9. Gong, C., et al.: An improved delay-suppressed sliding-mode observer for sensorless vector-controlled PMSM. IEEE Trans. Ind. Electron. 67(7), 5913–5923 (2020)
10. Yuan, Q., et al.: Low speed sensorless control based on an improved sliding mode observation and the inverter nonlinearity compensation for SPMSM. IEEE Access. 8, 61299–61310 (2020)
11. Bolognani, S., Oboe, R., Zigliotto, M.: Sensorless full-digital PMSM drive with EKF estimation of speed and rotor position. IEEE Trans. Ind. Electron. 46(1), 184–191 (1999)
12. Yang, H., et al.: FPGA-based sensorless speed control of PMSM using enhanced performance controller based on the reduced-order EKF. IEEE J. Emerg. Sel. Topics Power Electron, 1 (2019)
13. Holtz, J., Juliet, J.: Sensorless acquisition of the rotor position angle of induction motors with arbitrary stator windings. IEEE Trans. Ind. Appl. 41(6), 1675–1682 (2005)
14. Kim, S., Ha, J.I., Sul, S.K.: PWM switching frequency signal injection sensorless method in IPMSM. IEEE Trans. Ind. Appl. 48(5), 1576–1587 (2012)
15. Jansen, P.L., Lorenz, R.D.: Transducerless position and velocity estimation in induction and salient ac machines. IEEE Trans. Ind. Appl. 31(2), 240–247 (1995)
16. Briz, F., et al.: Comparison ofsaliency-based sensorless control techniques for AC machines. IEEE Trans. Ind. Appl. 40(4), 1107–1115 (2004)
17. Kim, D., et al.: Suppression of injection voltage disturbance for high-frequency square-wave injection sensorless drive with regulation of induced high-frequency current ripple. IEEE Trans. Ind. Appl. 52(1), 302–312 (2016)
18. Wang, G., et al.: Rotor position estimation of PMSM in low-speed region and standstill using zero-voltage vector injection. IEEE Trans. Power. Electron. 33(9), 7948–7958 (2018)
19. Wang, G., et al.: Sensorless control scheme of IPMSMs using HF orthogonal square-wave voltage injection into a stationary reference frame. IEEE Trans. Power Electron. 34(3), 2573–2584 (2019)
20. Fatu, M., et al.: I-F starting method with smooth transition to EMF based motion-sensorless vector control of PM synchronous motor/generator. In: 2008 IEEE Power Electronics Specialists Conference, pp. 1481–1487 (2008)
21. Wang, Z., Lu, K., Blaabjerg, F.: A simple startup strategy based on current regulation for back-EMF-based sensorless control of PMSM. IEEE Trans Power Electron. 27(8), 3817–3825 (2012)
22. Iepure, L.I., Boldea, I., Blaabjerg, F.: Hybrid I-f starting and observer-based sensorless control of single-phase BLDC-PM motor drives. IEEE Trans. Ind. Electron. 59(9), 3436–3444 (2012)
23. Tang, Q., Chen, D., He, X.: Integration of improved flux linkage observer and I–F starting method for wide-speed-range sensorless SPMSM drives. IEEE Trans. Power Electron. 35(8), 8374–8383 (2020)
24. Xing, J., et al.: Research on startup process for sensorless control of PMSMS based on I-F method combined with an adaptive compensator. IEEE Access. 8, 70812–70821 (2020)
25. Jansson, M., et al.: Synchronization at startup and stable rotation reversal of sensorless nonsalient PMSM drives. IEEE Trans. Ind. Electron. 53(2), 379–387 (2006)
26. Schmidt, P.B., et al.: Initial rotor angle detection of a nonsalient pole permanent magnet synchronous machine. In: IAS '97 Conference Record of the 1997 IEEE Industry Applications Conference Thirty-Second IAS Annual Meeting, 11, pp. 459–463 (1997)
27. Matsui, N.: Sensorless PM brushless DC motor drives. IEEE Trans. Ind. Electron. 43(2), 300–308 (1996)
28. Gardner, F.: Phaselock Technique, 3rd ed. Willey (2005)
29. Jeong, S.-G., Park, M.-H.: The analysis and compensation of dead-time effects in PWM inverters. IEEE Trans. Ind. Electron. 38(2), 108–114 (1991)
30. Raute, R., et al.: Analysis and compensation of inverter nonlinearity effect on a sensorless PMSM drive at very low and zero speed operation. IEEE Trans. Ind. Electron. 57(12), 4065–4074 (2010)
31. Gong, L.M., Zhu, Z.Q.: A novel method for compensating inverter nonlinearity effects in carrier signal injection-based sensorless control from positive-sequence carrier current distortion. IEEE Trans. Ind. Appl. 47(3), 1283–1292 (2011)
32. Han, J., Kim, B.-H., Sul, S.-k.: Effect of current measurement error in angle estimation of permanent magnet AC motor sensorless control. In: 2017 IEEE 3rd International Future Energy Electronics Conference and ECCE Asia (IFEEC 2017 - ECCE Asia), Kaohsiung, pp. 2171–2176 (2017)

How to cite this article: Wu X, Zhu Z, Wu Z. A new simplified fundamental model-based sensorless control method for surface-mounted permanent magnet synchronous machines. *IET Electr. Power Appl.* 2021;15:159–170. https://doi.org/10.1049/elp2.12022